

Published in final edited form as:

Mol Imaging Biol. 2014 February ; 16(1): 109–117. doi:10.1007/s11307-013-0664-5.

PET Imaging of Stroke-Induced Neuroinflammation in Mice Using [¹⁸F]PBR06

Frederick M. Lartey¹, G-One Ahn^{1,6}, Bin Shen³, Keith-Travis Cord¹, Tenille Smith^{4,9}, Joshua Y. Chua⁴, Sahar Rosenblum^{4,9}, Hongguang Liu³, Michelle L. James³, Sophia Chernikova¹, Star W. Lee^{1,4,8}, Laura J. Pisani³, Rabindra Tirouvanziam^{5,10}, John W. Chen⁷, Theo D. Palmer¹¹, Frederick T. Chin³, Raphael Guzman^{4,9}, Edward E. Graves^{1,2}, and Billy W. Loo Jr.^{1,2}

¹Department of Radiation Oncology, Stanford University School of Medicine, Stanford, CA, USA

²Stanford Cancer Institute, Stanford, CA, USA ³Department of Radiology, Stanford University

School of Medicine, Stanford, CA, USA ⁴Department of Neurosurgery, Stanford University School

of Medicine, Stanford, CA, USA ⁵Department of Pediatrics, Stanford University School of

Medicine, Stanford, CA, USA ⁶Integrative Biosciences & Biotechnology, Pohang University of

Science & Technology, Kyungbuk, 790-784, Korea ⁷Center for Systems Biology and Department

of Radiology, Massachusetts General Hospital, Harvard Medical School, Boston, MA, USA

⁸Laboratory of Genetics, The Salk Institute for Biological Studies, La Jolla, CA, USA

⁹Departments of Neurosurgery and Biomedicine, University of Basel, Basel, Switzerland

¹⁰Department of Pediatrics, Emory+Children's Center for CF Research, Emory University School

of Medicine, Atlanta, GA, USA ¹¹Institute for Stem Cell Biology and Regenerative Medicine,

Stanford University School of Medicine, Stanford, CA, USA

Abstract

Purpose—The purpose of this study is to evaluate the 18 kDa translocator protein (TSPO) radioligand [¹⁸F]*N*-fluoroacetyl-*N*-(2,5-dimethoxybenzyl)-2-phenoxyaniline ([¹⁸F]PBR06) as a positron emission tomography (PET) imaging biomarker of stroke-induced neuroinflammation in a rodent model.

Procedures—Stroke was induced by transient middle cerebral artery occlusion in Balb/c mice. Dynamic PET/CT imaging with displacement and preblocking using PK11195 was performed 3 days later. PET data were correlated with immunohistochemistry (IHC) for the activated microglial markers TSPO and CD68 and with autoradiography.

Results—[¹⁸F]PBR06 accumulation peaked within the first 5 min postinjection, then decreased gradually, remaining significantly higher in infarct compared to noninfarct regions. Displacement or preblocking with PK11195 eliminated the difference in [¹⁸F]PBR06 uptake between infarct and noninfarct regions. Autoradiography and IHC correlated well spatially with uptake on PET.

Conclusions— ^{18}F]PBR06 PET specifically images TSPO in microglial neuroinflammation in a mouse model of stroke and shows promise for imaging and monitoring microglial activation/neuroinflammation in other disease models.

Keywords

Stroke; Neuroinflammation; Translocator protein 18 kDa (TSPO); Peripheral benzodiazepine receptor (PBR); Positron emission tomography (PET); ^{18}F]PBR06

Introduction

Stroke is characterized by an inflammatory response that involves a variety of molecular, cellular, biochemical, and hormonal changes [1]. They include cytokine and chemokine-mediated activation of the brain's resident macrophages (microglia), upregulation of poly(ADP-ribose) polymerase-1, and multiple matrix metalloproteinases resulting in the disruption of the blood–brain barrier and the infiltration of neutrophils, and recruitment of macrophages and other leukocytes [2, 3]. Activated microglia release proinflammatory mediators and increase expression of immunomodulatory microglial proteins [4]. Among these proteins is the translocator protein-18 kDa (TSPO), previously referred to as the peripheral benzodiazepine receptor (PBR) [5]. This protein is located on the outer mitochondrial membrane of activated microglia and reactive astrocytes. TSPO expression is low in the healthy brain and increases markedly under neuroinflammatory conditions such as stroke. TSPO expression has thus been used as a biomarker of inflammation [6].

Multiple studies have identified numerous TSPO radioligands that can serve as positron emission tomography (PET) imaging agents for stroke and other inflammatory disorders [7]. These radioligands include ^{11}C]PK11195, ^{18}F]DPA-714, ^{11}C]DAA1106, ^{11}C]PBR28, ^{11}C]DAC, ^{18}F]FEAC, ^{18}F]FEDAC, and ^{18}F]FEDAA1106 [7–16]. Most have been used with varying degrees of success to image stroke in rats. The ^{18}F -labeled radioligand ^{18}F -*N*-fluoroacetyl-*N*-(2,5-dimethoxybenzyl)-2-phenoxyaniline (^{18}F]PBR06) [17] was recently developed as a neuroimaging agent for TSPO. It belongs to the aryloxyanilide class of compounds. Compared to existing TSPO radioligands, ^{18}F]PBR06 is distinguished by a number of features: ease of preparation, long half-life due to its ^{18}F , insignificant defluorination, high diffusibility across the blood–brain barrier in monkey, high binding affinity for TSPO in rat and monkey, and high specificity for TSPO [17]. Furthermore, it has been characterized in the human brain, and its biodistribution and radiation dosimetry in humans have been evaluated [18, 19], facilitating translation of results to human subjects. Thus, ^{18}F]PBR06 is an attractive neuroimaging agent for investigating neuroinflammatory disorders in preclinical models. Although ^{18}F]PBR06 has been characterized in three species (mice, rats, and humans), only one study involved imaging a pathological condition (glioma), and it has not yet been used in animal or human models of stroke or other nonmalignant neuroinflammatory conditions. This study therefore seeks to characterize and validate ^{18}F]PBR06 PET imaging in a mouse stroke model.

Materials and Methods

Preparation of ^{18}F -PBR06 and PK11195

An automated TRACERlab FX_{F-N} radiosynthetic module (GE Medical Systems, USA) was used in the preparation of [^{18}F]PBR06 as previously reported [17]. Briefly, aqueous [^{18}F]fluoride ion (44,400 MBq; 200 mCi) was dried by cycles of addition and evaporation of acetonitrile (1 cycle, 1 ml), complexed with 18-Crown-6 (1.7 mg; 6.4 μmol)/ K_2CO_3 (0.44 mg; 3.2 μmol) and reacted with the precursor *N*-(2,5-dimethoxybenzyl)-2-bromo-*N*-(2-phenoxyphenyl)acetamide (0.5 mg in 0.5 ml acetonitrile) at 110 °C for 10 min. [^{18}F]PBR06 was purified by injection into a semipreparative Gemini C18 column (5 μm , 10 \times 250 mm; Phenomenex, Torrance, CA, USA) at 214 nm and eluted at 5 ml/min with a mixture of (A) 50 mM ammonium formate (pH 6) and (B) 50 mM ammonium formate in MeCN (25:75, v/v) according to the program 57 % B for 2 min, increasing to 62 % B over 8 min, and slowly increasing to 67 % B for 40 min. The fraction containing [^{18}F]PBR06 (t_R =40 min) was collected in water (20 ml). This solution was passed through a C-18 Sep-Pak, and the trapped [^{18}F]PBR06 was eluted with ethanol (1 ml) and saline (9 ml) into a sterile flask. Typically, 592–1,480 MBq (16–40 mCi) of [^{18}F]PBR06 (>99 % chemically and radiochemically pure) was obtained with specific radioactivity ranging from 67 to 130 GBq/ μmol (1,800–3,500 mCi/ μmol) within 80–90 min (high-performance liquid chromatography purification and SepPak-based formulation included). Overall, radiochemical yield was 2.1 ± 0.7 % ($n=10$), and specific radioactivity was 98 ± 31 GBq/ μmol ($2,640 \pm 832$ mCi/ μmol) ($n=10$), both decay-corrected to the end of synthesis. For the displacement and preblocking studies, PK11195 (3.4 mg, Sigma-Aldrich, St. Louis, MO, USA) was dissolved in 1 ml ethanol, after which Tween 80 (15 mg) was added. The mixture was put in an ultrasonic bath for 5 min, and then 9 ml of saline was slowly added while stirring the solution. The final solution could be stored at room temperature for 2 h without precipitation.

Stroke procedure

Strokes were performed after approval by the Administrative Panel on Laboratory Animal Care of Stanford University. Three-month-old female Balb/c mice (Charles River Laboratories, Wilmington, MA, USA) were used. All strokes were induced by occluding the left middle cerebral artery (MCA) with a suture for 30 min using a previously described technique [20]. The mice were maintained under anesthesia with 2 % isoflurane for the entire procedure. A 5–0 silk suture was used to ligate the left external carotid artery, and a 7–0 monofilament suture was threaded into the left common carotid artery (CCA) until it encountered appropriate resistance indicating occlusion of the MCA. After 30 min, the monofilament was removed, and the CCA was permanently occluded with 5–0 silk suture. A total of nine mice identified on MRI as having clear infarcts were used in the studies, seven for the PET-CT imaging and two for the autoradiography studies.

MR imaging

Two days after stroke induction, high-resolution MRI was acquired on a 7-T animal MRI scanner (microSigna, GE Healthcare, Waukesha, WI, USA) equipped with a 9-cm bore gradient insert (Resonance Research, Inc., Billerica, MA, USA) and the LX11 control console (GE Healthcare, Waukesha, WI, USA). The radiofrequency coil used was an in-

house 1.5 cm diameter transmit–receive surface coil. The MRI acquisition included a T2-weighted (T2w) fast spin echo sequence with fat saturation (TE, 47.3 ms; TR, 4,000 ms; bandwidth, ± 15.6 kHz; echo train length, 8; slice thickness, 0.5 mm; number of slices, 32; FOV, 3 cm; acquisition matrix, 256×256 ; scan time, 4 min 56 s), acquired in the coronal plane.

PET/CT imaging

PET imaging was performed 3 days after stroke induction with a MicroPET R4 rodent model instrument (Siemens Medical Solutions Inc., Knoxville, TN, USA). The mice were anesthetized with 2 % isoflurane in oxygen and their tail veins catheterized. Custom tail vein catheters with a 40- μ L dead volume were constructed by connecting a 27-Ga butterfly needle to a 27-Ga hypodermic needle using a 10-cm length of 0.28 \times 0.61 mm polyethylene tubing (BD Diagnostics, Sparks, MD, USA). Four attached fiducial markers were applied for coregistration of PET with computed tomography (CT). Each marker was constructed from a microcentrifuge tube containing a drop of 0.037 MBq (1 μ Ci) of [18 F]PBR06 in 5 μ L of an iodinated CT contrast agent at its tip.

In the baseline study, four mice were injected (i.v.) with an average of 10.1 MBq (272 μ Ci) of [18 F]PBR06 (range, 9.5 MBq/258 μ Ci to 10.6 MBq/287 μ Ci) and dynamically scanned over an 80-min period, simultaneously in a four-mouse holder. In the displacement study, three of these mice were subsequently injected with 2 mg/kg of PK11195 and imaged for another 30 min. In the preblocking study, three additional mice were injected (i.v.) with PK11195 (2 mg/kg) 10 min prior to administration of [18 F]PBR06 (average, 6.6 MBq/178.7 μ Ci; range, 4.6 MBq/125 μ Ci to 10.2 MBq/276 μ Ci). The dose of PK11195 was chosen to be approximately 2,000 times the mass of the imaging dose of [18 F]PBR06 to ensure adequate competition for binding sites.

Immediately after PET imaging, the holder containing the mice was transferred to a SPECT-CT scanner (Gamma Medica Ideas, Northridge, CA, USA) for CT imaging. The CT protocol used was as follows: number of projections, 256; current, 335 μ A; voltage, 75KV; reconstruction, 512 \times 512 \times 512 with 170 μ m isotropic voxels.

Image analysis

PET image reconstruction was performed using the ordered subsets expectation maximization 2D algorithm [21]. The voxel size for the R4 scanner was 0.845 \times 0.845 \times 1.211 mm. No attenuation correction was applied during the reconstruction, but impact on quantification was previously determined to be minimal in this system using the same multianimal holder [22]. Images from all three modalities were analyzed using RT_Image, an in-house software tool that was developed using the Interactive Data Language (IDL; ITT Visual Information Solutions, Boulder, CO, USA) for functional imaging analysis in radiation oncology and preclinical imaging research [23]. PET and CT images were coregistered using a rigid body transformation by point matching using the four PET/CT fiducial markers. CT and MR images were also coregistered using a rigid body transformation by point matching using intracranial anatomic landmarks visible on both modalities. Finally, MR and PET images were coregistered by propagation of the MR/CT

and CT/PET transformations, so that the registration accuracy was not limited by the lower resolution of PET. Based on the MR images, regions of interest (ROIs) were drawn on every slice to delineate the infarct and noninfarct (matching regions in the contralateral hemisphere) regions, forming three-dimensional volumes. Radioactivity values were expressed in units of percent injected dose per gram (%ID/g) and were decay-corrected.

Autoradiography

Frozen brain sections (-20°C , 100 μm thick) were cut using a Leica CM1950 cryostat (Leica Microsystems, Wetzlar, Germany) and placed on microscope slides (Fisher Scientific, Waltham, MA, USA). Starting at approximately 3 h after the original *in vivo* injection of [^{18}F]PBR06, the slides were applied to a phosphor storage screen inside a cassette overnight at 4°C . The images were developed using a Cyclone phosphor storage system (Perkin Elmer, Waltham, MA, USA). Two mice were used for autoradiography.

Immunohistochemistry

Immunohistochemistry (IHC) for TSPO and CD68 (a specific marker for activated microglia) was performed as follows: The mice were euthanized with carbon dioxide, perfused with phosphate-buffered saline (PBS), and then fixed with paraformaldehyde. The brains were then harvested and kept at 4°C in 30 % sucrose overnight and subsequently placed in OCT (Sakura Fintek, Torrance, CA, USA). They were stored at -80°C until sectioning. Two adjacent sections (30 μm) from each brain were stained: the first with fluorescent dye-labeled antibody and the second with biotin-labeled antibody. The primary antibodies used were the following: the rabbit polyclonal anti-mouse antibody, NP155, an antibody against TSPO [24] provided by Dr. Makoto Higuchi of the National Institute of Radiological Sciences, Japan; and rat monoclonal anti-mouse CD68 (Abcam, Cambridge, MA, USA), both diluted at 1:1,000 in the blocking solution. The secondary antibodies used were goat antirat IgG Alexa Fluor 488 (Invitrogen, Carlsbad, CA, USA), goat antirabbit IgG Alexa Fluor 594 (Invitrogen, Carlsbad, CA, USA), and biotinylated antimouse IgG (Vector Laboratories, Burlingame, CA, USA). The staining procedures were based on standard IHC techniques for floating sections. Briefly, the first set of sections was placed in PBS containing NH_4Cl (50 mmol/l) for 5 min and then transferred to chilled methanol–acetone (1:1 at -20°C) for 5 min, followed immediately by Triton-X 100 (0.1 % in PBS) for 5 min. Blocking was performed with goat serum (5 %/Tween 0.5 %) in PBS for 30 min and immediately incubated with the primary antibodies at room temperature for 1 h followed by incubation with a fluorescent dye-labeled secondary antibody, also for 1 h. The sections were washed extensively with PBS after every step. They were then mounted in DAPI-containing medium and imaged with a laser scanning confocal microscope (Carl Zeiss Inc., Oberkochen, Germany). Adjacent sections were incubated with biotinylated secondary antibody coupled with streptavidin-horseradish peroxidase and reacted with 3,3'-diaminobenzidine (DAB). For these sections, prior to blocking, the endogenous peroxidase was quenched by incubating with a solution of hydrogen peroxide (30 %), methanol, and PBS in a 1:3:6 ratio at room temperature for 15 min. The secondary antibody used was a goat biotinylated anti-IgG in blocking solution. After secondary antibody incubation, the sections were immersed in avidin–biotin complex solution (Vector Laboratories, Burlingame, CA, USA) at room temperature for 30 min, placed in DAB solution (Vector

Laboratories, Burlingame, CA, USA) and mounted in water. The sections were washed in between steps with PBS and were visualized with an Olympus NanoZoomer 2.0-RS slide scanner (Center Valley, PA, USA). All seven mice that underwent PET imaging were further processed for IHC.

Statistical analysis

Statistical analysis was performed using GraphPad Prism software (GraphPad Software Inc., La Jolla, CA, USA). The Mann–Whitney test was used to compare the regions of interest within the stroke and non-stroke hemispheres. $P < 0.05$ indicated a statistically significant difference.

Results

Uptake of [^{18}F]PBR06 on PET

In all seven mice, MRI demonstrated left hemispheric infarcts covering regions in the cortex and in the adjacent striatal area (Fig. 1). PET demonstrated increased [^{18}F]PBR06 uptake corresponding to these regions (Fig. 2a). Time–activity curves demonstrated differential uptake profiles between infarct regions compared to noninfarct regions (Fig. 2b and Table 1). The tracer rapidly accumulated in the noninfarct regions, peaking by 5 min p.i., then clearing rapidly. In contrast, [^{18}F]PBR06 accumulation in the infarct regions was more gradual, peaking at 10 min, then clearing more gradually such that it was higher than in the noninfarct regions beyond 15 min p.i. By 60 min, the relative increase in uptake in the infarct regions stabilized, reaching 65 % higher in the infarct regions, than in the matching noninfarct regions.

Displacement and preblocking

To demonstrate that [^{18}F]PBR06 specifically binds TSPO *in vivo*, unlabeled PK11195 was used to either competitively displace [^{18}F]PBR06 from its binding site (displacement) or to competitively inhibit [^{18}F]PBR06 from binding to TSPO (preblocking study). From 5 min before to 5 min after displacement with PK11195 (2 mg/kg), [^{18}F]PBR06 uptake in the infarct cortex decreased from 73 to 17 %, respectively, above the matching noninfarct regions (Table 2). Corresponding values for the infarct striatum were 41 and 13 % (Table 2 and Fig. 3). While [^{18}F]PBR06 uptake was significantly higher in the infarct compared to noninfarct regions of the brain before displacement with PK11195, there was no longer any significant difference after displacement (Table 2). Of note, the initial rise in uptake in all regions after displacement represents redistribution of displaced tracer systemically from nonbrain tissues.

Preblocking with PK11195 (2 mg/kg) eliminated the difference in uptake between the infarct regions and the matching noninfarct regions (Table 3 and Fig. 4). At 60 min p.i., the uptake in the infarct cortex and striatum was 1.7 and 2.5 %ID/g, respectively, or 63 and 76 % of the uptake in the corresponding regions of animals without preblocking (Table 3).

Autoradiography

Figure 5 shows representative autoradiographic images demonstrating intense focal uptake of [^{18}F]PBR06 in regions corresponding to those of increased uptake demonstrated by PET/CT imaging and to the infarct regions identified by MRI. Mean radioactivity for the infarct increased by 190 % over the corresponding region in the noninfarct hemisphere.

Immunohistochemistry

As demonstrated by IHC, there was intense CD68 expression in the left hemisphere corresponding to the infarct regions as identified on T2w MRI and to the areas of highest [^{18}F]PBR06 uptake on PET (Fig. 6a). In the infarct region, immunofluorescence staining demonstrates that large numbers of activated microglia indicated by CD68 staining coexpress TSPO, whereas they are nearly absent in the noninfarct region (Fig. 6b).

Discussion

Several PET imaging agents have been studied as markers of microglial neuroinflammation after stroke in human and animal models [10, 14, 15, 25, 26]. In the present study, we have expanded upon these existing findings through evaluation of the recently developed radiotracer [^{18}F]PBR06 and correlation with multimodal imaging and histology. [^{18}F]PBR06 offers several practical advantages associated with ^{18}F -labeled radioligands over ^{11}C -labeled ones, particularly when considering eventual clinical translation: The longer half-life allows for imaging at centers remote from the cyclotron and allows more flexible and consistent scheduling, and the relatively high spatial resolution of the new generation of PET scanners is better realized owing to the lower-energy positron produced by the [^{18}F]fluoride ion [17].

The low resolution of PET compared to other imaging modalities, particularly in a small animal model, makes quantification challenging as regions of interest are difficult to define. Even with CT coregistration, infarct regions in individual animals are not well delineated. In addition, the stroke procedure itself is technically demanding and can produce infarcts of variable sizes. We performed MRI confirmation of infarcts in each animal. In addition, we performed PET-CT-MR image registration and MR-guided delineation of infarct regions of interest in each animal. This permitted infarct region specific quantification of tracer uptake on PET. In contrast to this study, the PET images from prior studies were registered with an MRI template of the rat brain [25, 26] or with the MRI of a normal rat brain, rather than MRI for the individual animals [14, 15].

To our knowledge, this study represents the first report of micro-PET imaging of microglial activation in a mouse stroke model. Compared to rats, a practical advantage of the mouse model is their smaller size and the ability to image multiple animals simultaneously in the same scanner making larger imaging studies more efficient. A challenge given the low resolution of PET is the smaller brain size, which makes it difficult to identify the infarct and surrounding regions. For this reason, MR-based ROI definition is of particular value in this animal model. This novel approach now offers the capability to perform longitudinal studies in gene knockout and reporter mouse models. Studies focused on the significance of

poststroke microglial activation, and the role of anti-inflammatory pathways could lead to new interventions to ameliorate stroke-related morbidity. With respect to the [^{18}F]PBR06 tracer, we have demonstrated an increased uptake in infarct regions compared to corresponding regions in the noninfarct hemisphere, competitively inhibiting the uptake of [^{18}F]PBR06 by pretreating the mouse with PK11195, or by displacing the tracer with PK11195, diminished the accumulation and uptake ratio significantly, demonstrating that the tracer binds specifically to TSPO in the mouse stroke model. Of note, the preblocking and displacement studies demonstrate binding specificity using both inter-animal (preblocking) and intra-animal (displacement) comparisons. The initial increase in uptake immediately following displacement may be attributed to release from TSPO in peripheral sites [27]. In addition, immediately after injection, [^{18}F]PBR06 signal was initially lower in the infarct compared to comparable regions on the contralateral hemisphere. This could have been caused by perfusion compromise in the necrotic brain parenchyma and a higher heterogeneity of capillary concentration in the infarct regions resulting in compromised microcirculation and a reduction in uptake of the radiotracer within the infarct [28]. Tracer uptake in the ventral portion the brain was high, apparently “penumbra” from inflammatory activity in the adjacent pharyngeal structures. These areas were excluded from the regions of interest for analysis as described in the methods.

IHC indicated that TSPO was expressed in higher concentration in the infarct and confirmed that the increased accumulation of [^{18}F]PBR06 in the infarct was due to an increased expression of TSPO. It has been hypothesized that the neuronal lesions in the infarct trigger TSPO expression in the microglia [29]. Increased microglial TSPO expression is part of a general neuroinflammatory response to brain injury during which activation of microglia and macrophage recruitment from the blood occurs. In the current study, staining with a second antibody specific for CD68, a distinct microglial biomarker, indicated that there was an increased activation of microglia in the infarct regions. The pattern of expression was similar to those from both the MRI and PET images. Furthermore, the staining pattern demonstrated by laser scanning confocal microscopy showed substantial overlap of TSPO and CD68. This suggests that antibodies to TSPO and CD68 were staining activated microglia in the infarct regions. The results in this study thus indicate that [^{18}F]PBR06 accumulates at the site of increased TSPO protein concentration in the infarct regions as a result of the increased activation of microglia. The classical TSPO ligand [^{11}C]PK11195 has been used in various studies to image stroke in rodents and humans. However, the limitations of [^{11}C]PK11195 have been well documented and include being highly lipophilic, having a lower binding affinity for TSPO, and a relatively short half-life. Consequently, as many as 40 ligands that target TSPO have been developed for PET imaging [30]. Previous studies suggest that TSPO activation in cells is maximum 11 days after stroke induction [31]. In studies with [^{11}C]PK11195, increased activity could not be clearly discerned in the infarct region, relative to the noninfarct region of the rat brain, 1–3 days after stroke induction [26]. A subsequent study, also in rats using [^{18}F]DPA-714, reported that the time of maximum radioligand uptake was 11 days after stroke induction [25]. Radioligand accumulation at day 4 poststroke induction was reported to be significantly lower than at day 11. This study demonstrates that in contrast to [^{11}C]PK11195, [^{18}F]PBR06 significantly accumulates in the infarct regions 3 days

poststroke induction. Further studies will use this tracer to characterize the time course of stroke progression in mice over time in the same animal using our tracer, as has recently been done using a novel MRI-based inflammation imaging agent [32]. The present study demonstrated the ability to image stroke 3 days after induction in mice. With its high binding affinity for TSPO, high ratio of TSPO-specific to nonspecific binding, easy preparation, and lack of defluorination, [^{18}F]PBR06 offers a promising alternative to [^{11}C]PK11195 in PET imaging of TSPO. Moreover, since characterization of the tracer has already been performed in humans, there is a high potential for rapid translation to imaging of stroke in human subjects.

Our study has several limitations. Although an advantage of using the mouse model is the ability to image a larger number of animals in parallel for greater efficiency, the smaller brains make quantitation of subvolumes more challenging given the low spatial resolution of PET. This highlights the importance in this case of defining the regions of interest based on higher resolution MRI. Even so, the quantitation is still limited by the lower underlying resolution of PET. Furthermore, the differences we observed, while statistically significant because of the intense neuroinflammation produced by stroke, were based on a small number of animals. In particular, the autoradiography study included only two mice. A larger number of animals would increase the power to distinguish smaller differences in uptake when studying more subtle inflammatory processes. Finally, the imaging time point of 3 days poststroke was chosen based on our prior observation of the presence of intense inflammation at that time, but it may not be the optimal time point to study. Future studies will image [^{18}F]PBR06 longitudinally after stroke along with quantitative functional/behavioral and immunohistochemical correlates and will evaluate the impact of anti-inflammatory interventions on these measurements.

Conclusions

In this study, we validated [^{18}F]PBR06 as a PET radioligand for imaging microglial neuroinflammation in a mouse model of stroke by demonstrating that: (1) [^{18}F]PBR06 uptake on PET and autoradiography is increased in regions corresponding to infarcts identified on MRI; (2) its uptake can be competitively inhibited by PK11195, indicating that its binding is reversible and specific to the same binding site (TSPO); (3) microglial activation is present in the same anatomic regions as increased [^{18}F]PBR06 uptake, as demonstrated by IHC for CD68; and (4) activated microglia observed in these studies exhibit increased TSPO expression as demonstrated by IHC showing colocalization of TSPO with CD68, and indicating that this is the source of increased [^{18}F]PBR06 uptake on PET imaging. As initial characterization of [^{18}F]PBR06 in human healthy volunteers has been performed, this agent is a promising candidate for imaging stroke-induced neuroinflammation in humans.

Acknowledgments

The authors thank Dr. Victor W. Pike and the National Institute of Mental Health for providing the [^{18}F]PBR06 precursor and standard, Dr. Makoto Higuchi of the National Institute of Radiological Sciences, Japan, for providing the TSPO antibody and the Stanford Center for Innovation in In Vivo Imaging. The study was supported in part by a Bio-X Interdisciplinary Initiatives Program (IIP) award from Stanford University (to BWL), a Developmental Cancer Research Award (DCRA) in Translational Research from Stanford Cancer Institute (to BWL), a NCI

ICMIC P50 award (CA114747 to Dr. Sanjiv Sam Gambhir), an American Heart Association Grant (AHA-0835274 N to RG), a CIRM grant (RC1-0134 to TDP), grants from the National Research Foundation of Korea and the Ministry of Education, Science and Technology, Korea (R31-10105 and NRF-2012M3A9C6049796 to G-OA), and the Department of Radiation Oncology, Stanford University.

References

1. Wang Q, Tang XN, Yenari MA. The inflammatory response in stroke. *J Neuroimmunol.* 2007; 184:53–68. [PubMed: 17188755]
2. Milner R. Microglial expression of alphavbeta3 and alphavbeta5 integrins is regulated by cytokines and the extracellular matrix: beta5 integrin null microglia show no defects in adhesion or MMP-9 expression on vitronectin. *Glia.* 2009; 57:714–723. [PubMed: 18985734]
3. Coull BM. Inflammation and stroke—introduction. *Stroke.* 2007; 38:631–631.
4. Weinstein JR, Koerner IP, Moller T. Microglia in ischemic brain injury. *Future Neurol.* 2010; 5:227–246. [PubMed: 20401171]
5. Papadopoulos V, Baraldi M, Guilarte TR, et al. Translocator protein (18 kDa): new nomenclature for the peripheral-type benzodiazepine receptor based on its structure and molecular function. *Trends Pharmacol Sci.* 2006; 27:402–409. [PubMed: 16822554]
6. Rupprecht R, Papadopoulos V, Rammes G, et al. Translocator protein (18 kDa) (TSPO) as a therapeutic target for neurological and psychiatric disorders. *Nat Rev Drug Discov.* 2010; 9:971–988. [PubMed: 21119734]
7. Cagnin A, Kassiou M, Meikle SR, Banati RB. Positron emission tomography imaging of neuroinflammation. *Neurotherapeutics.* 2007; 4:443–452. [PubMed: 17599710]
8. Fujimura Y, Hwang PM, Trout H Iii, et al. Increased peripheral benzodiazepine receptors in arterial plaque of patients with atherosclerosis: an autoradiographic study with [(3)H]PK 11195. *Atherosclerosis.* 2008; 201:108–111. [PubMed: 18433754]
9. Fujimura Y, Ikoma Y, Yasuno F, et al. Quantitative analyses of ¹⁸F-FEDAA1106 binding to peripheral benzodiazepine receptors in living human brain. *J Nucl Med.* 2006; 47:43–50. [PubMed: 16391186]
10. Gerhard A, Neumaier B, Elitok E, et al. *In vivo* imaging of activated microglia using [¹¹C]PK11195 and positron emission tomography in patients after ischemic stroke. *Neuroreport.* 2000; 11:2957–2960. [PubMed: 11006973]
11. James ML, Fulton RR, Henderson DJ, et al. Synthesis and *in vivo* evaluation of a novel peripheral benzodiazepine receptor PET radioligand. *Bioorg Med Chem.* 2005; 13:6188–6194. [PubMed: 16039131]
12. Imaizumi M, Kim HJ, Zoghbi SS, et al. PET imaging with [¹¹C]PBR28 can localize and quantify upregulated peripheral benzodiazepine receptors associated with cerebral ischemia in rat. *Neurosci Lett.* 2007; 411:200–205. [PubMed: 17127001]
13. James ML, Fulton RR, Vercoullie J, et al. DPA-714, a new translocator protein-specific ligand: synthesis, radiofluorination, and pharmacologic characterization. *J Nucl Med.* 2008; 49:814–822. [PubMed: 18413395]
14. Yui J, Maeda J, Kumata K, et al. ¹⁸F-FEAC and ¹⁸F-FEDAC: PET of the monkey brain and imaging of translocator protein (18 kDa) in the infarcted rat brain. *J Nucl Med.* 2010; 51:1301–1309. [PubMed: 20660373]
15. Yui J, Hatori A, Kawamura K, et al. Visualization of early infarction in rat brain after ischemia using a translocator protein (18 kDa) PET ligand [¹¹C]DAC with ultra-high specific activity. *Neuroimage.* 2011; 54:123–130. [PubMed: 20705143]
16. Ikoma Y, Yasuno F, Ito H, et al. Quantitative analysis for estimating binding potential of the peripheral benzodiazepine receptor with [¹¹C]DAA1106. *J Cereb Blood Flow Metab.* 2007; 27:173–184. [PubMed: 16685259]
17. Briard E, Zoghbi SS, Simeon FG, et al. Single-step high-yield radiosynthesis and evaluation of a sensitive ¹⁸F-labeled ligand for imaging brain peripheral benzodiazepine receptors with PET. *J Med Chem.* 2009; 52:688–699. [PubMed: 19119848]

18. Fujimura Y, Zoghbi SS, Simeon FG, et al. Quantification of translocator protein (18 kDa) in the human brain with PET and a novel radioligand, (18)F-PBR06. *J Nucl Med.* 2009; 50:1047–1053. [PubMed: 19525468]
19. Fujimura Y, Kimura Y, Simeon FG, et al. Biodistribution and radiation dosimetry in humans of a new PET ligand, ¹⁸F-PBR06, to image translocator protein (18 kDa). *J Nucl Med.* 2010; 51:145–149. [PubMed: 20008980]
20. Mao Y, Yang GY, Zhou LF, Stern JD, Betz AL. Focal cerebral ischemia in the mouse: description of a model and effects of permanent and temporary occlusion. *Brain Res Mol Brain Res.* 1999; 63:366–370. [PubMed: 9878831]
21. Hudson HM, Larkin RS. Accelerated image reconstruction using ordered subsets of projection data. *IEEE Trans Med Imaging.* 1994; 13:601–609. [PubMed: 18218538]
22. Habte, FRG.; Doyle, T.; Cheng, Z.; Gambhir, S.; Paik, D. High-throughput multiple mice imaging on microPET and microPET-CT scanners: evaluation on image quantitation effect. *World Molecular Imaging Congress; San Diego:* 2011.
23. Graves EE, Quon A, Loo BW Jr. RT_Image: an open-source tool for investigating PET in radiation oncology. *Technol Cancer Res Treat.* 2007; 6:111–121. [PubMed: 17375973]
24. Ji B, Maeda J, Sawada M, et al. Imaging of peripheral benzodiazepine receptor expression as biomarkers of detrimental versus beneficial glial responses in mouse models of Alzheimer's and other CNS pathologies. *J Neurosci.* 2008; 28:12255–12267. [PubMed: 19020019]
25. Martin A, Boisgard R, Theze B, et al. Evaluation of the PBR/TSPO radioligand [¹⁸F]DPA-714 in a rat model of focal cerebral ischemia. *J Cereb Blood Flow Metab.* 2010; 30:230–241. [PubMed: 19794397]
26. Rojas S, Martin A, Arranz MJ, et al. Imaging brain inflammation with [¹¹C]PK11195 by PET and induction of the peripheral-type benzodiazepine receptor after transient focal ischemia in rats. *J Cereb Blood Flow Metab.* 2007; 27:1975–1986. [PubMed: 17457364]
27. Boutin H, Chauveau F, Thominiaux C, et al. ¹¹C-DPA-713: a novel peripheral benzodiazepine receptor PET ligand for *in vivo* imaging of neuroinflammation. *J Nucl Med.* 2007; 48:573–581. [PubMed: 17401094]
28. Vogel J, Hermes A, Kuschinsky W. Evolution of microcirculatory disturbances after permanent middle cerebral artery occlusion in rats. *J Cereb Blood Flow Metab.* 1999; 19:1322–1328. [PubMed: 10598936]
29. Van Camp N, Boisgard R, Kuhnast B, et al. *In vivo* imaging of neuroinflammation: a comparative study between [¹⁸F]PBR111, [¹¹C]CLINME and [¹¹C]PK11195 in an acute rodent model. *Eur J Nucl Med Mol Imaging.* 2010; 37:962–972. [PubMed: 20069292]
30. Dolle F, Luus C, Reynolds A, Kassiou M. Radiolabelled molecules for imaging the translocator protein (18 kDa) using positron emission tomography. *Curr Med Chem.* 2009; 16:2899–2923. [PubMed: 19689272]
31. Maeda J, Higuchi M, Inaji M, et al. Phase-dependent roles of reactive microglia and astrocytes in nervous system injury as delineated by imaging of peripheral benzodiazepine receptor. *Brain Res.* 2007; 1157:100–111. [PubMed: 17540348]
32. Breckwoldt MO, Chen JW, Stangenberg L, et al. Tracking the inflammatory response in stroke *in vivo* by sensing the enzyme myeloperoxidase. *Proc Natl Acad Sci U S A.* 2008; 105:18584–18589. [PubMed: 19011099]

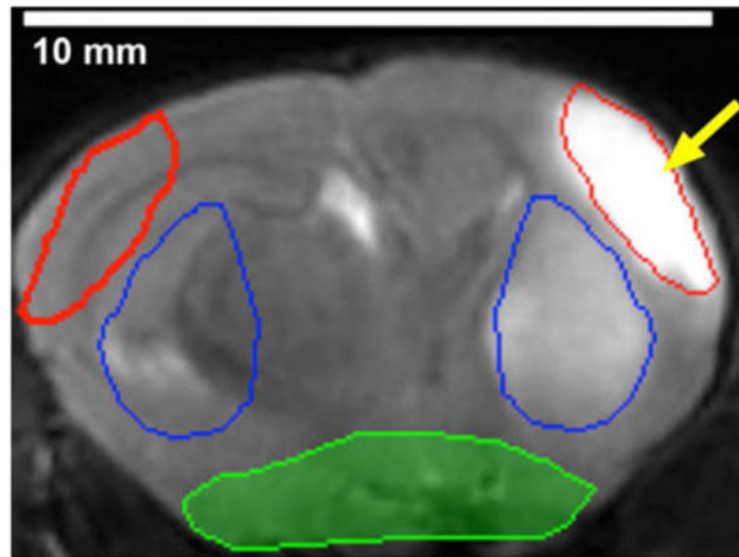


Fig. 1.

A representative MR image of the mouse brain showing the different regions of interest (ROI) used in the analysis. In the infarct hemisphere (*left hemisphere*), the red ROI delineates the cortical infarct region (*arrow*) and the blue ROI delineates the striatal infarct region. Copies of each ROI were reflected and placed in matching regions in the noninfarct hemisphere (*right hemisphere*). The *shaded region in green* was excluded to remove inflammatory signal from the adjacent pharynx from the analysis.

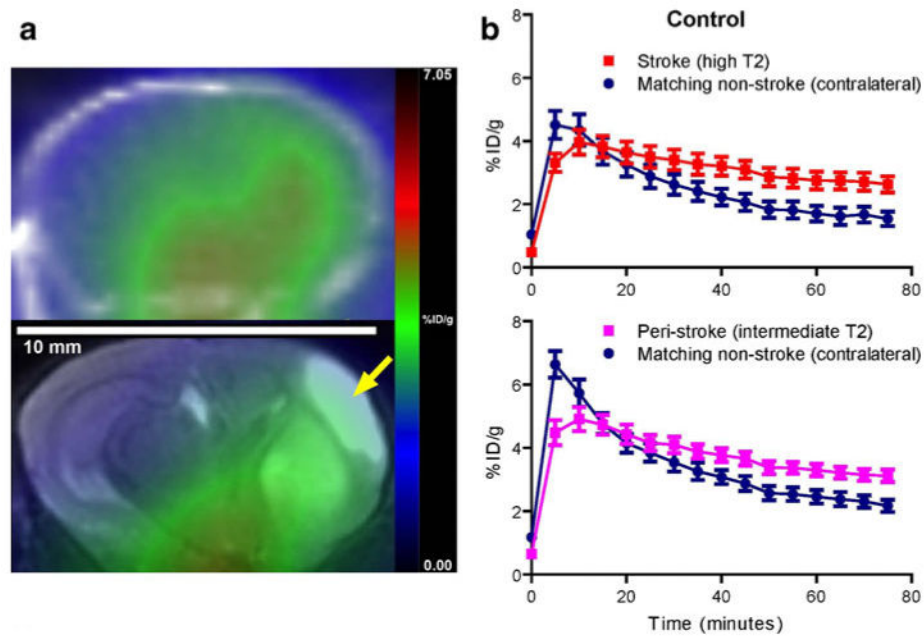


Fig. 2.
a Representative coregistered PET/CT (*top*) and PET/MR (*bottom*) coronal images of the infarct (*arrow*) and noninfarct hemispheres of the mouse brain after injection of [^{18}F]PBR06. The PET image represents a summation over 20 min of 1-min dynamic scans from 40 to 60 min postinjection. The cortical and striatal infarct regions of interest delineated on MRI are superimposed on both the PET/CT and PET/MR views of the same animal. **b** Time–activity curves of [^{18}F]PBR06 uptake in the cortex (*top*) and striatum (*bottom*) of the infarct as well as matching regions on the non-infarct hemisphere. Activity values are presented as mean \pm SEM.

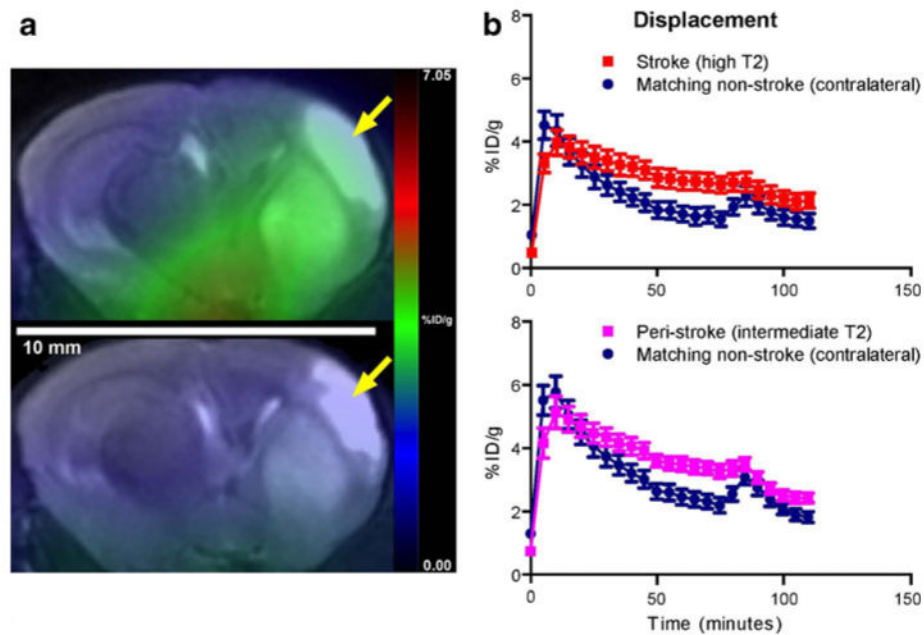


Fig. 3.
a Representative coregistered PET/CT coronal images of the infarct (*arrow*) and noninfarct hemispheres of the mouse brain before (*top*) and after (*bottom*) displacement with PK11195 in the same animal. The PET images represent summations over 20 min of 1 min dynamic scans from 40 to 60 min and 85 to 110 min after [^{18}F]PBR06 injection, respectively. **b** Time–activity curves showing the displacement of [^{18}F]PBR06 by PK11195 (at $t=80$ min, *arrow*) for the cortical and striatal infarct regions compared to matching regions on the noninfarct hemisphere, manifest as loss of separation between the curves after PK11195 injection. Activity values are presented as mean \pm SEM.

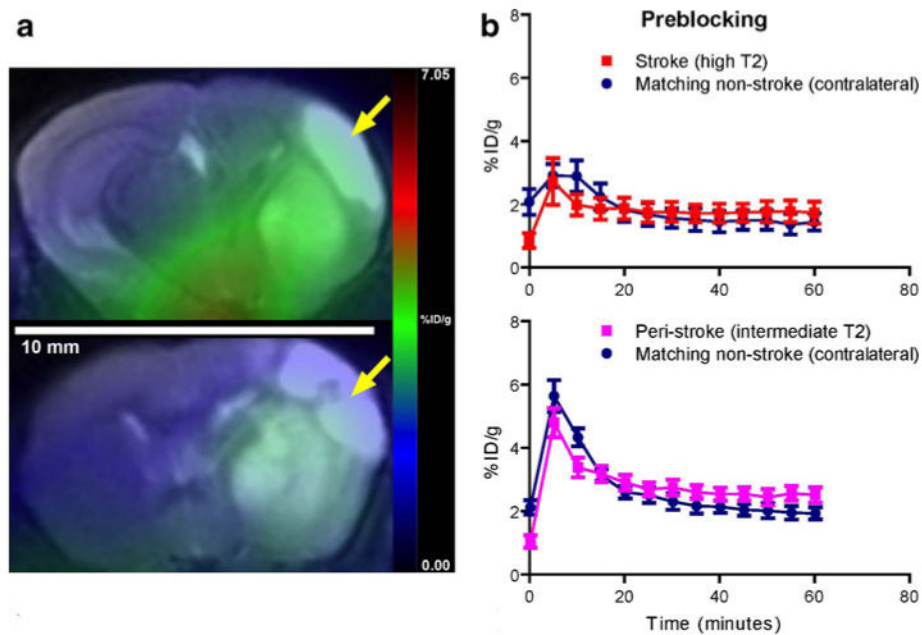


Fig. 4.
a Representative coregistered PET/CT coronal images of the infarct (*arrow*) and noninfarct hemispheres of the brains of a control mouse (*top*) and a different mouse after preblocking with PK11195 (*bottom*). The PET images for each mouse represent a summation over 20 min of 1 min dynamic scans from 40 to 60 min after [^{18}F]PBR06 injection. **b** Time-activity curves showing the blocking of [^{18}F]PBR06 by PK11195 for the cortical and striatal infarct regions compared to matching regions on the noninfarct hemisphere, manifest as lack of separation between the curves. Activity values are presented as mean \pm SEM.



Fig. 5. Autoradiography images from 100- μ m sections of the mouse brain demonstrate increased focal uptake of [^{18}F]PBR06 corresponding qualitatively to regions of increased uptake on PET imaging and increased T2-weighted signal on MRI.

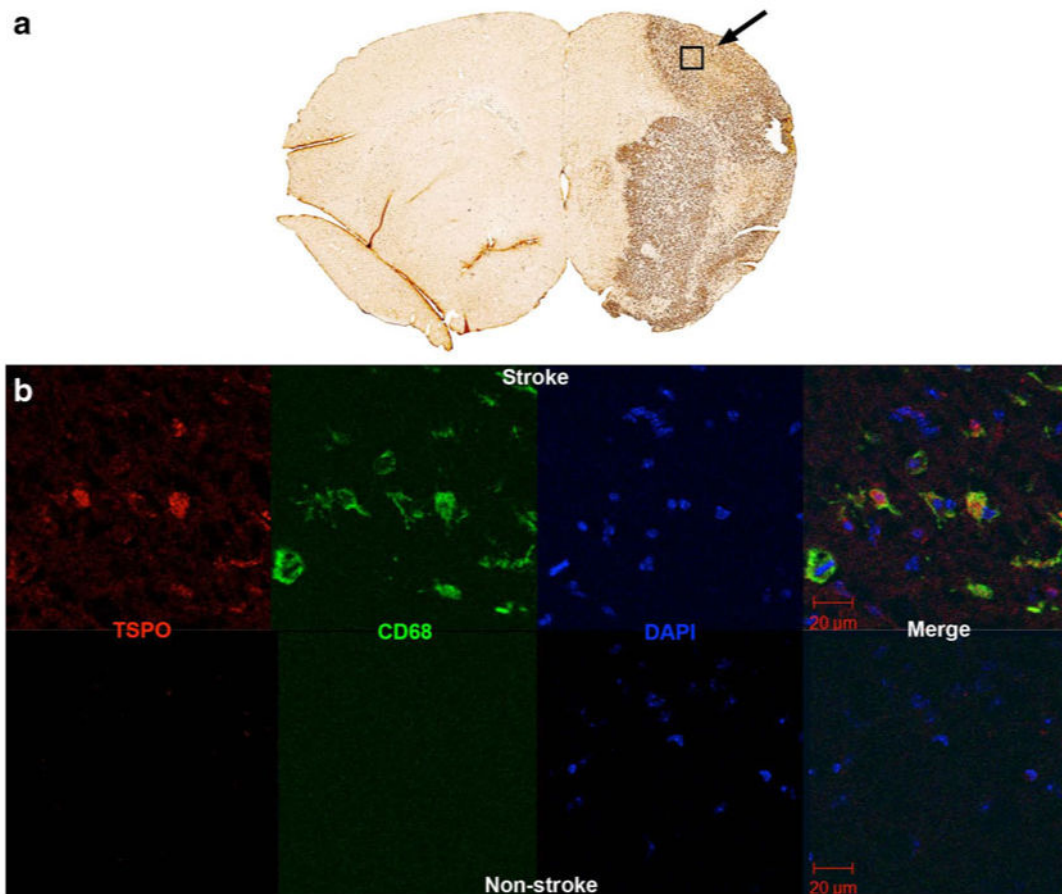


Fig. 6.

a CD68 immunohistochemistry demonstrates intense staining (*arrow*) indicating marked microglial activation in the regions corresponding to the cortical and striatal infarct seen on the T2-weighted MRI, and increased [^{18}F]PBR06 uptake on PET. The rectangle indicates the region on an adjacent section from which immunofluorescence images were obtained. **b** Immunofluorescence for TSPO and CD68, as well as nuclear staining with DAPI and merged images, of stroke (*top row*) and nonstroke (*bottom row*) regions. In the infarct region, large numbers of activated microglia indicated by CD68 staining coexpress TSPO, whereas they are nearly absent in the noninfarct region.

Table 1
Percentage increase in [¹⁸F]PBR06 in the cortex and striatum compared to matching contralateral regions over time

Time (min)	Activity (%ID/g)	Activity (%ID/g)	% Increase	P value
	Cortex	Contralateral region		
5	3.3±0.29	4.5±0.44	-26	0.017
10	4.0±0.40	4.3±0.50	-7	0.36
15	3.8±0.42	3.7±0.34	3	0.67
30	3.4±0.33	2.6±0.32	31	0.042
45	3.1±0.29	2.1±0.27	48	0.010
60	2.8±0.27	1.7±0.25	65	0.008
75	2.6±0.26	1.5±0.23	73	0.005
	Striatum	Contralateral region		
5	6.6±0.42	4.5±0.39	-32	0.003
10	5.7±0.43	4.9±0.38	-14	0.068
15	4.7±0.31	4.8±0.33	-2	0.89
30	4.1±0.26	3.5±0.29	17	0.070
45	3.7±0.22	2.9±0.23	28	0.013
60	3.3±0.21	2.4±0.20	38	0.007
75	3.1±0.20	2.2±0.20	41	0.004

The percentage increases in activities in the cortical and striatal infarct regions over those of matching contralateral nonstroke regions at various times after injection of [¹⁸F]PBR06. Activity values are presented as mean±SEM

Table 2
Differences in accumulation of [¹⁸F]PBR06 in the cortex and striatum compared to matching contralateral regions before and after displacement of [¹⁸F]PBR06 with PK11195

Time (min)	Activity (%ID/g)	Activity (%ID/g)	% Increase	P value
	Cortex	Contralateral region		
60	2.8±0.27	1.7±0.25	65	0.008
75	2.6±0.26	1.5±0.23	73	0.005
85	2.7±0.31	2.3±0.32	17	0.16
90	2.5±0.28	2.0±0.30	25	0.13
	Striatum	Contralateral region		
60	3.3±0.21	2.4±0.20	38	0.007
75	3.1±0.20	2.2±0.20	41	0.004
85	3.5±0.21	3.1±0.24	13	0.085
90	3.1±0.21	2.8±0.25	11	0.13

The percentage increases in activities in the cortical and striatal infarct regions over those of matching contralateral nonstroke regions immediately before and after displacement of [¹⁸F]PBR06 with PK11195 (at 80 min). Activity values are presented as mean±SEM

Table 3
Percentage changes in [¹⁸F]PBR06 in the cortex and striatum compared to matching contralateral regions in mice previously blocked with PK11195

Time (min)	Activity (%ID/g)	Activity (%ID/g)	% Increase	P value
	Cortex	Contralateral region		
5	2.7±0.73	2.9±0.36	-7	0.71
10	2.0±0.33	2.9±0.50	-31	0.058
15	1.8±0.34	2.2±0.41	-18	0.30
30	1.7±0.31	1.5±0.31	13	0.47
45	1.7±0.33	1.5±0.31	13	0.37
60	1.7±0.35	1.4±0.28	21	0.31
	Striatum	Contralateral region		
5	4.8±0.46	5.6±0.50	-16	0.099
10	3.4±0.31	4.3±0.28	-21	0.017
15	3.2±0.25	3.1±0.19	-3	0.82
30	2.7±0.24	2.3±0.26	17	0.095
45	2.5±0.21	2.0±0.19	20	0.038
60	2.5±0.24	1.9±0.19	24	0.031

The differences in activities of [¹⁸F]PBR06 in the cortical and striatal infarct regions over those of matching contralateral nonstroke regions in a mouse previously injected with PK11195. Activity values are presented as mean±SEM